

UvA-DARE (Digital Academic Repository)

Spectral Shaping by Radiative Energy Transfer in CsPbBr₃ Nanocrystal-Dye Mixtures

Flaucher, Ina; van der Laan, Marco; Huisman, Jef; Schall, Peter

DOI

[10.1021/acsaom.5c00098](https://doi.org/10.1021/acsaom.5c00098)

Publication date

2025

Document Version

Final published version

Published in

ACS Applied Optical Materials

License

CC BY

[Link to publication](#)

Citation for published version (APA):

Flaucher, I., van der Laan, M., Huisman, J., & Schall, P. (2025). Spectral Shaping by Radiative Energy Transfer in CsPbBr₃ Nanocrystal-Dye Mixtures. *ACS Applied Optical Materials*, 3(4), 1036-1043. <https://doi.org/10.1021/acsaom.5c00098>

General rights

It is not permitted to download or to forward/distribute the text or part of it without the consent of the author(s) and/or copyright holder(s), other than for strictly personal, individual use, unless the work is under an open content license (like Creative Commons).

Disclaimer/Complaints regulations

If you believe that digital publication of certain material infringes any of your rights or (privacy) interests, please let the Library know, stating your reasons. In case of a legitimate complaint, the Library will make the material inaccessible and/or remove it from the website. Please Ask the Library: <https://uba.uva.nl/en/contact>, or a letter to: Library of the University of Amsterdam, Secretariat, P.O. Box 19185, 1000 GD Amsterdam, The Netherlands. You will be contacted as soon as possible.

UvA-DARE is a service provided by the library of the University of Amsterdam (<https://dare.uva.nl>)

Spectral Shaping by Radiative Energy Transfer in CsPbBr₃ Nanocrystal–Dye Mixtures

Ina Flaucher,* Marco van der Laan, Jef Huisman, and Peter Schall*

Cite This: *ACS Appl. Opt. Mater.* 2025, 3, 1036–1043

Read Online

ACCESS |



Metrics & More



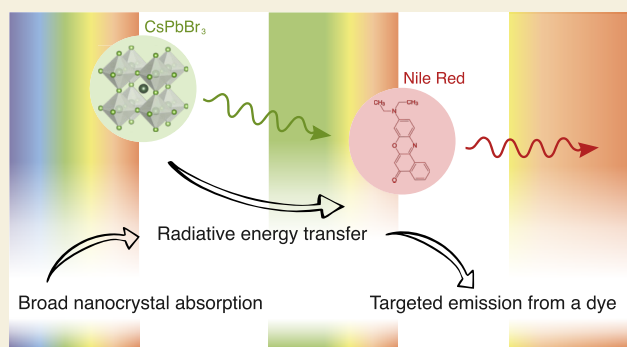
Article Recommendations



Supporting Information

ABSTRACT: Spectral shaping is a technique to spectrally focus the broadband solar spectrum for diverse energy conversion applications from luminescent solar concentrators to horticulture. Fluorescent dyes have been used as optically active components due to their high photoluminescence quantum yield (PLQY), but their absorption range is limited. Nanocrystals offer broadband absorption but are typically limited in spectral shifting, causing photon recycling. Here, we investigate radiative energy transfer from CsPbBr₃ nanocrystals to Nile Red dye, combining the nanocrystals' broadband absorption with the dye's targeted emission. We use experimental transmittance and (time-resolved) photoluminescence (PL) spectroscopy together with photon random walk simulations to show that indeed radiative energy transfer occurs and that the resulting extended absorption range due to the nanocrystals can significantly enhance the spectral conversion efficiency. Experimentally, the energy transfer manifests in PL excitation spectra as strongly enhanced absorption and in time-resolved PL as a prolonged rise and decay time, reflecting the delay due to the extra absorption and emission processes. The photon random walk simulations account for the observed spectra quantitatively and allow prediction of conversion spectra for a wide range of nanocrystal and dye concentrations as well as their material parameters such as the PLQYs of the components. Specifically, we highlight the role of competitive absorption and the importance of taking the spectral intensity profile of excitation light into account when quantifying broadband energy transfer. These results open the door to tuning of absorption and emission spectra via the design of optimized compound mixtures for targeted spectral shaping applications.

KEYWORDS: Radiative Energy Transfer, CsPbBr₃, Nile Red, Solution, Photon Random Walk, Concentration Dependence, Spectral Shaping, Compound Mixtures



INTRODUCTION

Sunlight, as the most abundant source of energy available, holds tremendous potential for meeting the world's growing energy needs.¹ Shaping its spectrum for diverse light-harvesting applications is a central goal to enhance conversion efficiencies and make the best possible use of the sun's energy. Spectral shaping uses fluorescent materials to modify the spectral distribution of light by converting parts of the spectrum to different wavelengths, weakening some spectral ranges, while intensifying others. Examples include applications in photovoltaic technologies, such as luminescent solar concentrators, designed to convert and direct light toward solar cells, thereby allowing the collection of radiation over a large area.² Another application area outside photovoltaics that is less explored but potentially offers great benefits is spectral shaping to enhance the photosynthesis of plants, offering great potential for increasing biomass quantity and quality.^{3,4} Photosynthesis relies on the absorption of specific wavebands of light via pigments within the photosynthetic apparatus, leaving the broad solar spectrum used rather inefficiently for photo-

synthetic energy conversion.^{5–7} Modern horticulture counters light deficiency through use of artificial lightening, adding well-tuned LED light to enhance and steer plant growth.^{8,9} Alternatively, the use of spectral shaping materials can provide a more sustainable approach, making best use of the sun's energy. By utilizing spectral shaping layers composed of fluorescent materials, natural sunlight can be adjusted to best suit the needs of plants without extra energy.

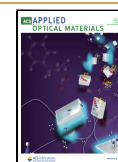
Previous work using molecular dyes has already shown promising results of enhanced plant growth by intensifying red light, which is typically absorbed particularly well by plants.¹⁰ Nevertheless, molecular dyes exhibit only relatively narrow absorption bands, limiting the broad spectral conversion.

Received: March 10, 2025

Revised: March 27, 2025

Accepted: March 27, 2025

Published: April 8, 2025



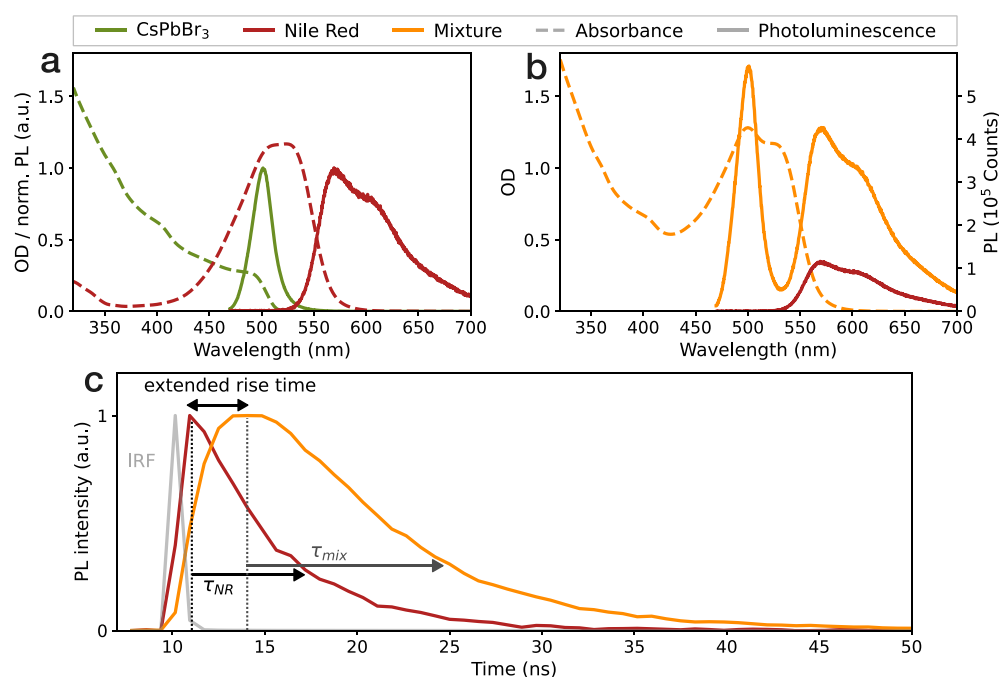


Figure 1. Optical properties of CsPbBr₃ nanocrystals and Nile Red dye. (a) Absorbance (optical density (OD), dashed lines) and photoluminescence (PL, solid lines) spectra of CsPbBr₃ nanocrystals and Nile Red dye, normalized to their respective maxima. The emission peak of the nanocrystals overlaps with the dye's absorption region. (b) Corresponding absorbance and PL spectrum of the nanocrystal–dye mixture (with the same material concentrations as in (a)). The PL spectrum of pure Nile Red dye (red line) is shown for comparison on the same (absolute) PL axis (right). PL spectra show strong enhancement of the Nile Red emission due to the addition of nanocrystals. All PL spectra were excited at 400 nm. (c) Time-resolved PL traces at 600 nm emission wavelength in the pure dye solution (red) and in the mixture with CsPbBr₃ (orange) excited at 375 nm. The mixture exhibits a prolonged rise and extended PL lifetime compared to those of the pure Nile Red sample. Arrows indicate the PL lifetimes $\tau_{NR} = 5.2$ ns and $\tau_{mix} = 9.9$ ns of Nile Red and the mixture, at which the PL intensity has decreased to 1/e of the maximum. The rise time from the center of the laser excitation to the center of maximum PL intensity is extended from 0.8 ns in the pure Nile Red sample to 3.85 ns in the mixture. The gray curve shows the instrumental response function (IRF).

Semiconducting nanocrystals can close this gap due to their continuum absorption above the bandgap, while exhibiting excellent photoluminescence quantum yields (PLQYs).¹¹ Yet, they often suffer from only a small spectral shift between their absorption and emission, called Stokes shift, causing internal light trapping due to reabsorption of the emitted light,^{12,13} thus limiting the spectral conversion tunability. Ultimately, the light trapping is caused by the radiative energy transfer between the nanocrystals. Although a mixture of nanocrystals could be used to funnel light to the desired spectral region, as long as the final emitter exhibits a small Stokes shift, the problem remains.

Combining the two classes of fluorescent materials, nanocrystals and dyes, in a simple mixture could significantly extend the light-conversion potential while maintaining the flexibility of spectral tuning. In such a mixture, radiative energy transfer, with nanocrystals serving as broadband absorber and molecular dyes serving as targeted emitter, would allow spectral shaping to be greatly enhanced and tuned, without chemical linking of the two components. Previous work has shown energy transfer between nanocrystals and molecular dyes achieved through direct coupling of the compounds, typically governed by Förster energy transfer^{14–25} or other nonradiative transfer mechanisms.^{23,26} In these cases, chemical coupling between the donor and acceptor is achieved through anchoring carboxylate or amine groups attached to the dye molecules, which are often Rhodamine-,^{14,16–19} perylene-,^{20,24} or cyanine^{21,26} based. While these studies demonstrate nonradiative energy transfer and evaluate its efficiency based on monochromatic excitation light, broadband excitation and

spectral tunability of the absorber and emitter side is important for many spectral conversion applications. The question is then whether radiative energy transfer in simple compound mixtures is sufficiently efficient to separate the absorption and emission processes onto two different fluorophores over a broad range of excitation wavelengths. If so, this would greatly enhance the spectral-shaping abilities for diverse application areas while shifting the chemical challenges of surface engineering in the case of nonradiative energy transfer to optical optimization for radiative energy transfer systems.

Here, we investigate energy transfer and its impact on the spectral shaping ability in a mixture of a molecular dye and semiconducting nanocrystals. Motivated by applications for cyanobacteria⁷ and plants,⁸ we focus on a mixture of perovskite nanocrystals (CsPbBr₃) and Nile Red, specifically exploring the impact of the broadband-absorbing nanocrystals on the spectral conversion of a white light source. We use the nanocrystals as absorbers for UV and blue light, providing green emission, which matches the green-light absorption of the Nile Red dye. The Nile Red dye serves as an ideal acceptor molecule for studying radiative energy transfer alone, as it lacks anchoring groups that would enable chemical coupling of the two components and nonradiative energy transfer.¹⁹ Using a combination of spectroscopic techniques and modeling, we find that indeed radiative energy transfer occurs from the nanocrystals to the dye and the broad UV-blue absorption of the nanocrystals significantly enhances the red light emission from Nile Red. We elucidate the dynamics of the energy transfer via time-resolved photoluminescence measurements,

exhibiting extended rise and decay times of the dye material in the presence of the nanocrystals. A photon random walk model is used to gain further insights into the energy transfer process. By extracting mean free path lengths of the two fluorophores from the experimental absorption spectra and using the experimentally measured photoluminescence quantum yields and emission profiles, we construct random walks of photons in the simulated mixture and compute the output spectrum, taking into account the geometrical boundary conditions. We apply this model to simulate the output converted spectra of the standard 1.5G solar spectrum for a wide range of nanocrystal and dye concentrations and show that the energy transfer can enhance the conversion efficiency by up to ~9% for unity PLQY nanocrystals. These results highlight the extended potential of spectral conversion through energy transfer upon mixing two different types of fluorophores and elucidate the critical interplay of absorption, energy transfer, and emission in the enhanced spectral conversion.

METHODS

We synthesized CsPbBr₃ nanocrystals with a PLQY of 70% following a slightly adapted method from Protesescu et al.¹¹ Nile Red powder was used as received and had a PLQY value of 71%. Both compounds were dissolved in toluene and stored in 10 × 10 mm, 3.5 mL quartz cuvettes. All measurements were performed using samples containing a concentration of 0.74 mg mL⁻¹ CsPbBr₃ nanocrystals or 10 μg mL⁻¹ Nile Red powder and their respective mixture.

We measured reference-corrected optical densities (ODs) with a LAMBDA 950 UV/vis/NIR spectrophotometer from PerkinElmer, and we measured photoluminescence spectra using a Fluorolog-3 instrument (HORIBA Jobin Yvon) coupled to a xenon lamp. Photoluminescence quantum yields were determined by using an integrating sphere (819C-IS-5.3 from Newport). Excitation was provided with a 150 W xenon lamp coupled to a M130 monochromator from Solar LS. Scattered, transmitted, and emitted photons were detected using a CCD camera (Hamamatsu S10141-1108S) coupled to a M266 monochromator from Solar LS. The spectral conversion measurements were performed using the same setup but with a broadband illumination from a Solux MR16 lamp mounted in front of the sphere with the front of it opened with a hole of 2 mm diameter. Time-resolved photoluminescence data was gathered using a LifeSpec II time-correlated single-photon counting spectrometer from Edinburgh Instruments. Excitation was realized with a 100 ps pulsed diode laser (EPL series) at 375 nm.

RESULTS

Absorption and emission spectra of perovskite CsPbBr₃ nanocrystals and Nile Red are shown in Figure 1a. The nanocrystals show broadband absorption below 500 nm and emission with a peak at 500 nm. We identify the typical overlap between absorption and emission spectra with a small Stokes shift toward the excitonic resonance at around 495 nm. The molecular dye Nile Red shows strong absorption from 450 to 560 nm, and an emission profile covering the range between 520 and 730 nm. By design, there is full spectral overlap between the nanocrystal emission and the dye absorption enabling energy transfer from CsPbBr₃ to Nile Red. We emphasize that the small Stokes shift of the nanocrystals can result in reabsorption of the emitted photons followed by re-emission by the nanocrystals themselves, a phenomenon called photon recycling, which typically lowers the PLQY.^{12,13} As this is especially observed for highly concentrated samples, we ensured that our measurements were conducted within a concentration range where photon recycling is negligible.¹² For the Nile Red dye, this overlap of its absorption and emission

bands is small, minimizing photon recycling within this compound. We also note that the flat background in the absorption spectra at wavelengths longer than the absorption edges indicates a low amount of scattering for both samples.

After the two solutions were mixed in a 1:1 ratio, the absorption and emission spectra display optical characteristics of both, as shown in Figure 1b. At low concentrations, the relation between concentration and OD is linear and the OD of the mixture is the sum of the ODs of the separate compounds. We have chosen an excitation wavelength of 400 nm to measure the photoluminescence (PL) spectra, where Nile Red shows poor direct absorption and most of the light is absorbed by the nanocrystals. Nevertheless, in the PL of the mixture, we still observe a strong increase of the Nile Red emission, indicating that energy is transferred from the CsPbBr₃ nanocrystals to Nile Red. At the same time, we observe no spectral shift in the emission or absorption profiles of donor and acceptor material, which would result from a direct chemical coupling of the two materials,^{14,18–20} indicating the energy transfer occurs between the dispersed fluorophores, as intended. Finally, the presence of green emission reveals that, despite the energy transfer, a significant portion of the nanocrystal emission is not absorbed by the dye and escapes the nanocrystal–dye mixture. See Figure S2 in the Supporting Information for all raw photoluminescence data.

To further confirm the energy transfer from CsPbBr₃ to Nile Red, we performed time-resolved photoluminescence (TRPL) measurements. We track the time-dependent PL intensity of the dye at 600 nm and observe two significant changes from the pure Nile Red to the mixed sample: (i) a prolonged rise time and (ii) an extended decay time in the presence of the nanocrystals (see Figure 1c). In the pure sample, the emission intensity rises within 0.8 ns upon laser excitation, while in the mixture, the rise is delayed and the center of maximum fluorescence intensity is reached only after ~3.85 ns, which is on the order of the nanocrystal PL decay time of 5.85 ns. The 1/e PL decay time of Nile Red extends from 5.2 ns in the pure sample to 9.9 ns in the mixture, indicating a longer PL lifetime of the dye in the mixture, as highlighted with τ_{mix} versus τ_{NR} in the figure. We note that the PL decay of the dye in the mixture resulting from the energy transfer cannot be adequately described by a simple exponential decline due to the continuous radiative decay of the nanocrystals over the period of the nanocrystal decay time (~6 ns). Taken together with the change in emission intensities, we thus conclude that energy transfer occurs in the mixture. The prolonged rise time then suggests that a radiative process underlies this energy transfer, as nonradiative transfer processes typically occur within hundreds of picoseconds.^{14,22,23} In nonradiative transfer systems, PL lifetimes consequently also increase by at most several hundred picoseconds.²² In our case, photons emitted by CsPbBr₃ are subsequently absorbed and re-emitted by Nile Red, explaining the extended lifetime. The radiative nature of the process is further corroborated by looking at the typical nanocrystal–dye distances within the mixture: from the number density of nanocrystals of 1.52×10^{14} mL⁻¹, we estimate that, on average, a CsPbBr₃ nanocrystal can be found every 104 nm, while Nile Red molecules with a number density of 1.89×10^{16} mL⁻¹ are found every 21 nm, yielding typical nanocrystal–dye distances of several tens of nanometers. Nonradiative energy transfer would typically require donor–acceptor distances of 5 to 8 nm.²⁷ We also looked at the full distance distribution and found that, for randomly placed

nanocrystals and dyes at the given densities, only a small fraction of nanocrystal–dye pairs (<3%) has a distance close enough (<8 nm) for efficient Förster energy transfer, as shown in the Supporting Information.

The advantage of the nanocrystal addition is that it extends the range of excitation to shorter wavelengths compared to that of the dye alone. To probe this enhanced excitation range directly, we use photoluminescence excitation (PLE) measurements to scan over the excitation wavelength while tracking the Nile Red emission intensity at a fixed wavelength of 600 nm. The resulting PLE spectrum of the mixture reveals a clear PL intensity enhancement for excitation wavelengths between 320 nm and ~470 nm, as shown in Figure 2a. In contrast, within

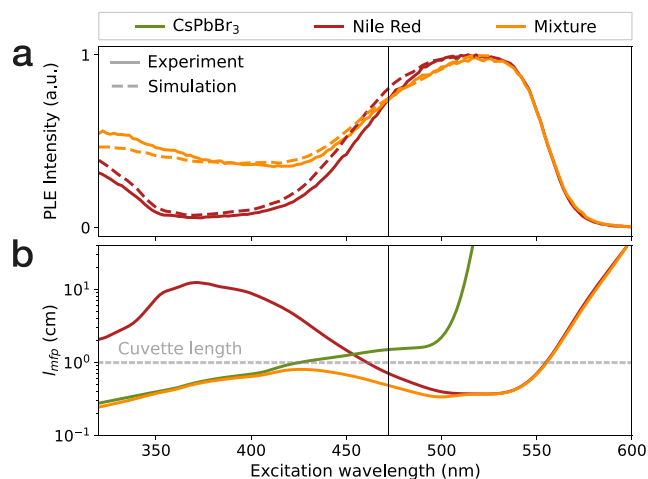


Figure 2. Photoluminescence excitation spectra and mean free path lengths. (a) Photoluminescence excitation (PLE) spectra at 600 nm emission of Nile Red (solid red line) and the CsPbBr₃–Nile Red mixture (solid orange line). Simulated PLE spectra, obtained by integration over a 560–700 nm emission wavelength range, are shown as dashed lines. Data have been normalized to the simulated Nile Red intensity at 520 nm. (b) Mean free path length (l_{mfp}) of photons traveling through the sample. Cuvette length is indicated by a gray dotted line. Vertical black line delineates crossover from emission enhancement to emission loss due to nanocrystals at ~470 nm.

the dye’s absorption band from ~470 to 600 nm, the PL intensity is nearly unaltered, suggesting that, here, direct excitation of the dye dominates and the addition of nanocrystals does not lead to an enhancement. We ascribe the slight reduction of the emission intensity for excitation wavelengths between ~470 and ~525 nm to the competitive absorption of the nanocrystals, whose nonunity PLQY reduces the efficiency of indirect excitation compared to the direct dye excitation. To further elucidate the contributions of the two components, we extract the mean free path lengths l_{mfp} of photons from the measured optical densities (Figure 1b) via

$$l_{\text{mfp}}(\lambda) = -\frac{d}{\log_{10}(10^{-OD(\lambda)})} \quad (1)$$

The resulting wavelength-dependent mean free path length is shown in Figure 2b. The gray dotted line represents the cuvette length $d = 1$ cm; l_{mfp} values exceeding 1 cm indicate that photons are unlikely to interact with the medium and therefore are more likely to be transmitted through the sample.

For the Nile Red sample, the mean free path length at wavelengths below ~450 nm is much longer than the cuvette

length, reflecting the low absorption of Nile Red alone. With the addition of CsPbBr₃, the mean free path length significantly shortens, indicating enhanced absorption due to the nanocrystals. At longer wavelengths between ~460 and 550 nm, coinciding with the dye’s absorption band, l_{mfp} in the Nile Red sample shortens to below the cuvette length, resulting in a strong interaction, whereas, upon exceeding the CsPbBr₃ absorption edge at 500 nm, the mean free path of the CsPbBr₃ sample grows rapidly and exceeds the cuvette length, suppressing absorption by the nanocrystals. For wavelengths just below the absorption edge of the CsPbBr₃ nanocrystals at 500 nm, both materials compete for the incoming photons. The CsPbBr₃ nanocrystals and the Nile Red dye then act as competing absorbers, which results in a slight reduction of the PLE intensity in the mixture compared to that of the dye alone (see Figure 2a).

To obtain microscopic insight into the energy transfer processes and their spectral contributions, we modeled the light interaction of the mixture using a photon random walk model. The model includes absorption, emission, and scattering of photons by the nanocrystals and the dye, as shown in Figure 3a. These basic light–matter interactions naturally capture radiative energy transfer from the nanocrystals to the dye and eventual photon recycling within the nanocrystals. The photon trajectories are modeled in a simulated cuvette, taking into account reflection of light at the solvent–air interface due to the refractive-index contrast, which we assume to be constant over the entire wavelength range. To quantitatively incorporate the cross sections for absorption and scattering, we extract the mean free path lengths from the transmittance data (see Figure 2b), and to quantitatively incorporate the PL emission, we use the measured PLQY of the individual compounds. We then computed the total light emitted from the cuvette by integrating the photons escaping through any of the cuvette boundaries.

We first validate the accuracy of the model by computing transmission spectra, which we compare with the experimental transmittance shown in Figure 3b. Excellent overlap of the simulated and experimental curve is observed. As this transmittance spectrum is based on the mean-free paths length derived from the individual experimental transmittances of the two compounds, good overlap is expected, yet it shows that our assumptions in incorporating the reflection, scattering, and absorption processes in the cuvette geometry are valid. We can now use the model to simulate the emitted light spectrum according to any spectral input. We take the white-light spectrum of a Solux lamp, which provides a simple proxy for the solar spectrum in the lab, and use the model to compute the total modulated light spectrum. The computed spectrum is compared to the experimentally measured spectrum in Figure 3c. The latter has been taken using an integrating sphere to collect the light emitted in all directions, in line with our model calculations. The resulting emission spectra show a broadband intensity reduction for wavelengths shorter than 550 nm, in agreement with the absorption spectrum of the nanocrystal–dye mixture (Figure 1b), followed by an enhancement of the red spectral components between 560 and 700 nm. The simulation effectively captures both the shape and magnitude of the red light with a reasonable degree of accuracy. Some deviation is observed at ~500 nm, where the model overestimates the direct light emitted from the nanocrystals, possibly due to the simplified assumption of a two-dimensional

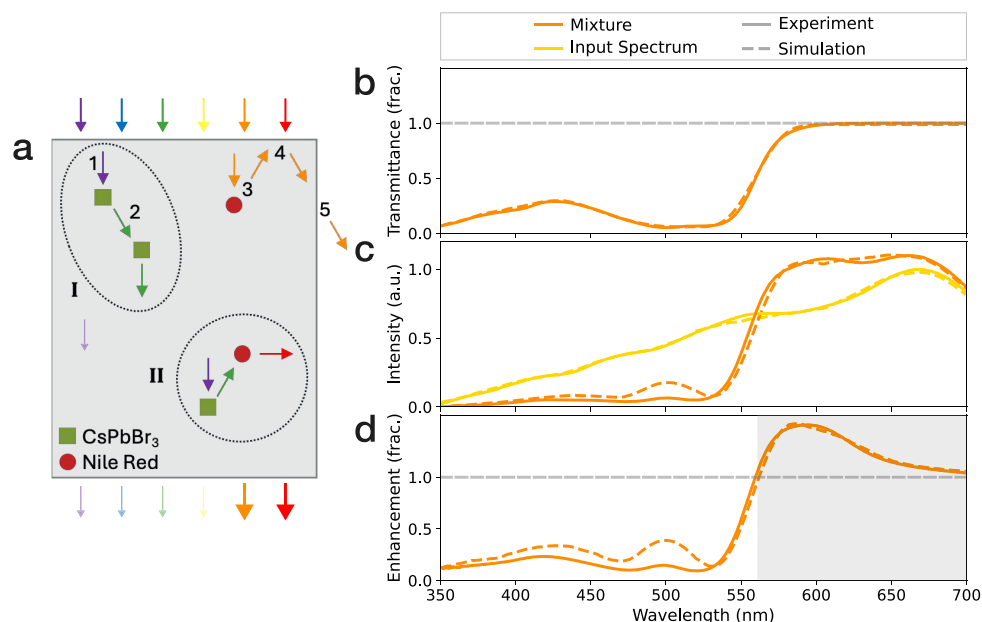


Figure 3. Photon random walk model. (a) Schematic of the optical processes included in the model: absorption (1), emission (2), scattering (3), reflection (4), and transmission (5). Photons enter the cuvette (gray box) at the top and interact with the CsPbBr₃ nanocrystals (green squares) and Nile Red dye (red circles). Light–matter interactions can result in I: photon recycling (successive emission and reabsorption by the nanocrystals); II: radiative energy transfer (emission by a nanocrystal and subsequent absorption by the dye). (b) Overlapping simulated (dashed lines) and experimental (solid lines) transmittance of the mixture indicates an accurate simulation approach for absorption, scattering, and reflection. (c) Spectral modification (orange curve) of a white-light spectrum (yellow curve) occurred upon interaction with the mixture. Simulations are in reasonable agreement with experimental data. (d) Enhancement ratio of the nanocrystal–dye mixture obtained by dividing the output by the input spectrum. Good overlap of the experimental and model data is observed. Gray shading delineates the Nile Red emission range.

geometry. Overall, the nanocrystal–dye mixture successfully converts large parts of the blue–green spectrum into the red spectral region. To show this most clearly and determine the spectral shaping efficiency, we divide the output by the input spectrum to define a fractional enhancement ratio. This ratio, plotted as a function of wavelength in Figure 3d, accentuates the output spectrum, with respect to the incident light spectrum. Values above 1 indicate an intensity increase due to the light conversion, while values below 1 indicate a reduction due to absorption. Clearly, much of the light below ~550 nm is absorbed and converted into light of ~560–700 nm wavelength, as shown consistently by both measurement and model results.

To explore the full potential of the nanocrystal–dye mixture for the spectral conversion of sunlight, we take the AM1.5G solar spectrum as input and vary the relative amounts of nanocrystals and dye to assess which composition gives the strongest spectral conversion. For each concentration ratio, we compute the output spectra and enhancement ratios (see Figure S3a,b in the Supporting Information). We define a single number characterizing the spectral shaping efficiency (SE) by integrating the intensity of the output spectrum over the wavelength range of 560–700 nm, corresponding to the Nile Red emission (gray area in Figure 3d), and divide this by the integrated intensity of the incident spectrum in the same wavelength range (see eq S7 in the Supporting Information for details).

Using this number, we can then map the spectral shaping efficiency as a function of nanocrystal and dye concentrations using the model. A map of the spectral shaping efficiency as a function of the concentration of both components is shown in Figure S4 in the Supporting Information. We find shaping efficiencies of up to 1.55, depending on the concentrations of

the two compounds. To highlight the nanocrystal contribution to the spectral shaping enhancement, we show the relative gain in shaping efficiency due to the nanocrystal presence in Figure 4. This map, which represents the relative difference between the shaping efficiency of the mixture and that of the dye alone

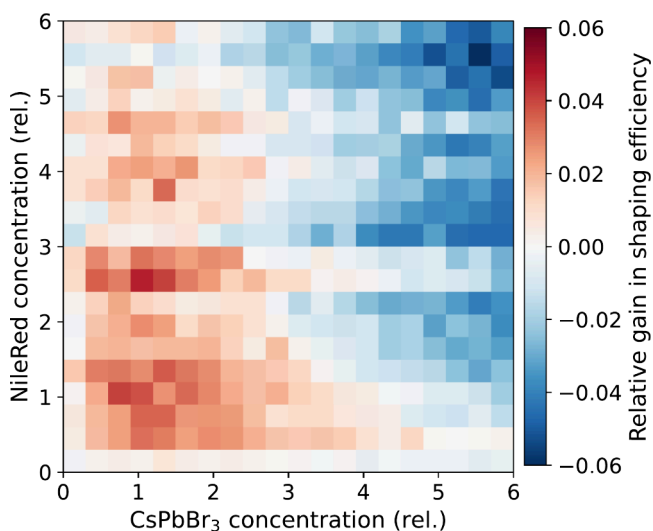


Figure 4. Relative gain in shaping efficiency of the nanocrystal–dye mixture. Map of the relative gain in shaping efficiency due to the presence of nanocrystals (i.e., the relative difference in shaping efficiency between the nanocrystal–dye mixture and the dye alone) as a function of the Nile Red dye and nanocrystal concentration. We find a relative gain enhancement of up to 5% for optimal nanocrystal–dye concentrations, based on a PLQY of our CsPbBr₃ nanocrystals of 70%.

(see eq S8 in the Supporting Information for details), elucidates the concentration dependence of the radiative energy transfer: at low to moderate concentrations, the addition of nanocrystals can lead to up to 5% gain due to their light absorption and energy transfer to the dye. Overall, this enhancement diminishes with an increasing concentration of the nanocrystals and of the dye. For the nanocrystals, this decrease in the shaping efficiency gain is related to competing absorption between the two compounds. As the nanocrystal concentration increases, both the initial absorption of excitation light and the chances of reabsorption of green emission within the nanocrystals become enhanced. Consequently, at high concentration, the nanocrystals critically dominate the absorption in the wavelength range of 450–500 nm and effectively reduce the overall red light emission.

Using the model, we can fully disentangle the contributions of the different excitation wavelengths to the total shaping efficiency. We vary the incident wavelength and compute, for each excitation wavelength, the resulting red emission from the converted spectrum. To enable comparison with the measured PLE spectra, we show the modeled red emission intensity as a function of the excitation wavelength in Figure 2a. Here, we have normalized the curve height to the simulated Nile Red emission intensity for excitation at 520 nm, as the simulations collect the emitted photons from the full space angle, unlike the PLE experiments, for which the limited collection angle is unknown. Good overlap with the experimental PLE spectra is observed for both the Nile Red and the mixture, further validating the correspondence between experiments and simulations.

To evaluate the spectral contributions to the shaping efficiency, we use the PLE spectra with and without nanocrystals to determine the gain in efficiency upon adding the nanocrystals as a function of excitation wavelength, as shown in Figure 5 (see eq S9 in the Supporting Information for details). The solid and dashed lines indicate, respectively, experimental and simulated data for the CsPbBr₃ PLQY value of 70%, while the shaded area indicates the simulated range in efficiency gain for PLQY values from 50% to 100%.

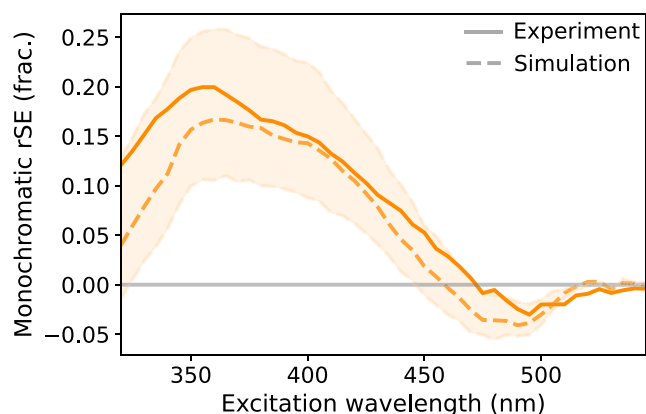


Figure 5. Spectrally resolved shaping efficiency. Monochromatic relative gain in shaping efficiency (rSE) as a function of excitation wavelength for experimental (solid line) and simulated (dashed line) nanocrystal–dye mixtures with nanocrystal PLQY of 70%. The orange-shaded region indicates the range of shaping efficiencies expected for nanocrystal PLQYs from 50% (lower bound) to 100% (upper bound). Experimental rSEs were obtained from the experimental PLE curves; see the text.

Interestingly, depending on the excitation wavelength, the addition of nanocrystals can both enhance and reduce the shaping efficiency. For light with wavelengths between 350 and 460 nm, which is poorly absorbed by the Nile Red, the nanocrystals are beneficial: their broadband absorption and subsequent energy transfer to Nile Red leads to an absolute efficiency enhancement of ~20% or up to 25% for nanocrystals with PLQY nearing 100%. In contrast, for wavelengths in the absorption region of Nile Red (between 460 and 520 nm), the nanocrystals have a rather negative influence: as the direct absorption and emission by Nile Red is more efficient than the two-step absorption via the nanocrystals, their addition decreases the shaping efficiency. The overall shaping efficiency gain thus depends on the incident light spectrum; spectra with sufficiently intense UV and blue light benefit from the addition of nanocrystals. For the AM1.5G solar spectrum and our nanocrystal PLQY of 0.7, we find that the conversion efficiency is enhanced by 5.3% for incident wavelengths between 300 and 460 nm, while it is decreased by 1.2% for longer wavelengths, leading to an overall gain of 4.1% due to the addition of nanocrystals. For unity PLQY values, the unfavorable wavelength range minimizes and an overall relative gain of up to ~8.8% can be obtained for the current concentration ratio (see Table S1 in the Supporting Information for more details).

Hence, depending on the input spectrum, the nanocrystal–dye mixture can be optimized. The photon random walk model then allows simulation of conversion efficiencies for a wide range of relative concentrations and nanocrystal PLQY values, which are experimentally time-consuming to obtain. By using the model to find the optimal concentration ratio for the AM1.5G solar spectrum and unity quantum yield of the nanocrystals, we calculate that the amount of red light between 560 and 700 nm can be enhanced by up to 9% using a concentration of 1.8 times the experimental concentration for both the nanocrystals and the Nile Red dye. In addition, as real incident sunlight varies throughout the day and year, one could use this model to systematically investigate spectral conversion as a function of the sunlight variability.

DISCUSSION AND CONCLUSION

We investigated, by spectroscopic measurements and simulations, the role of radiative energy transfer between CsPbBr₃ nanocrystals and the Nile Red dye for spectral shaping applications. The significant spectral overlap of nanocrystal emission and dye absorption enables energy transfer from CsPbBr₃ acting as donor material to Nile Red acting as acceptor, effectively enhancing its absorption over a broad range of UV-blue excitation wavelengths. This is confirmed in steady-state PL measurements that show enhanced Nile Red emission in the presence of the nanocrystals. Time-resolved PL measurements reveal elongated rise and decay times, suggesting that energy transfer in this study is primarily of radiative nature. In contrast, previous work has shown that nanocrystal–dye chemical binding through anchoring groups ensures close donor–acceptor distances and typically leads to nonradiative energy transfer occurring on shorter time scales and resulting in only modest lifetime increases.^{14,22,23} Already an earlier study by Muthu et al. examined energy transfer in a similar system (MAPbBr₃ and Nile Red) and observed minimal radiative transfer, likely due to low component concentrations and larger donor–acceptor distances. In contrast, our investigation at 37× higher donor and 53× higher acceptor concentrations reveals robust energy transfer,

suggesting that exploring this previously unexamined high-concentration regime enables effective radiative energy transfer.¹⁹

While the efficient energy-transfer process makes the contribution of the broadband-absorbing nanocrystals quite significant, the benefit strongly depends on the incident spectrum. Spectral shaping of two-component mixtures involves an intricate trade-off between enhancement due to the nanocrystals' additional absorption range and loss due to their competing absorption in the absorption regime of the dye. Therefore, under broadband white-light illumination, the impact of an additional absorbing material strongly depends on its PLQY and the overlap of its absorption spectrum with the absorption spectrum of the other component in the mixture. Our results suggest that for optimal nanocrystal–dye concentrations and unity nanocrystal quantum yields a shaping efficiency gain of up to 9% can be achieved, meaning that there are 9% more red photons in the output spectrum of the mixture than in that of Nile Red alone. Moreover, we note that we have included only the red emitted light in the shaping efficiency; the directly emitted green light from the nanocrystals can clearly also have a positive influence, depending on the photosynthetic species at hand.²⁸ The good agreement between measurements and photon random walk simulations suggests that the model can be used to evaluate numerous binary mixtures to find the best conversion efficiency for various applications using only experimental PLQY values and absorption/PL spectra of the components as input.

■ ASSOCIATED CONTENT

SI Supporting Information

The Supporting Information is available free of charge at <https://pubs.acs.org/doi/10.1021/acsaoam.5c00098>.

Synthesis details; data processing details; radiative versus nonradiative energy transfer; photon random walk model design; definitions of shaping efficiencies; figures of raw PL data, simulated conversion spectra, and concentration dependent shaping efficiencies; simulation results on relative shaping efficiencies for varying nanocrystal quantum yields (PDF)

■ AUTHOR INFORMATION

Corresponding Authors

Ina Flaucher – Institute of Physics and Department of Freshwater and Marine Ecology, Institute for Biodiversity and Ecosystem Dynamics, University of Amsterdam, Amsterdam 1098 XH, The Netherlands; orcid.org/0009-0001-2863-8095; Email: i.j.flaucher@uva.nl

Peter Schall – Institute of Physics, University of Amsterdam, Amsterdam 1098 XH, The Netherlands; orcid.org/0000-0003-2612-2762; Email: p.schall@uva.nl

Authors

Marco van der Laan – Institute of Physics, University of Amsterdam, Amsterdam 1098 XH, The Netherlands; orcid.org/0000-0001-9571-3190

Jef Huisman – Department of Freshwater and Marine Ecology, Institute for Biodiversity and Ecosystem Dynamics, University of Amsterdam, Amsterdam 1098 XH, The Netherlands

Complete contact information is available at:

<https://pubs.acs.org/doi/10.1021/acsaoam.5c00098>

Notes

The authors declare no competing financial interest.

■ ACKNOWLEDGMENTS

We thank Dr. Yingying Tang for providing the CsPbBr₃ nanocrystals. We thank the Science & Design programme of the FNWI (Faculteit der Natuurwetenschappen, Wiskunde en Informatica, University of Amsterdam) for funding this research.

■ REFERENCES

- (1) Kabir, E.; Kumar, P.; Kumar, S.; Adelodun, A. A.; Kim, K.-H. Solar energy: Potential and future prospects. *Renewable and Sustainable Energy Reviews* **2018**, *82*, 894–900.
- (2) Papakonstantinou, I.; Portnoi, M.; Debije, M. G. The Hidden Potential of Luminescent Solar Concentrators. *Adv. Energy Mater.* **2021**, *11*, No. 2002883.
- (3) Shen, L.; Yin, X. Solar spectral management for natural photosynthesis: from photonics designs to potential applications. *Nano Convergence* **2022**, *9*, 36.
- (4) Wondraczek, L.; Batentschuk, M.; Schmidt, M. A.; Borchardt, R.; Scheiner, S.; Seemann, B.; Schweizer, P.; Brabec, C. J. Solar spectral conversion for improving the photosynthetic activity in algae reactors. *Nat. Commun.* **2013**, *4*, 2047.
- (5) Fleming, G. R.; Schlau-Cohen, G. S.; Amarnath, K.; Zaks, J. Design principles of photosynthetic light-harvesting. *Faraday Discuss.* **2012**, *155*, 27–41.
- (6) Scholes, G. D.; Fleming, G. R.; Olaya-Castro, A.; van Grondelle, R. Lessons from nature about solar light harvesting. *Nat. Chem.* **2011**, *3*, 763–774.
- (7) Luimstra, V. M.; Schuurmans, J. M.; Verschoor, A. M.; Hellingwerf, K. J.; Huisman, J.; Matthijs, H. C. Blue light reduces photosynthetic efficiency of cyanobacteria through an imbalance between photosystems I and II. *Photosynthesis Research* **2018**, *138*, 177–189.
- (8) Zhang, M.; Whitman, C. M.; Runkle, E. S. Manipulating growth, color, and taste attributes of fresh cut lettuce by greenhouse supplemental lighting. *Scientia Horticulturae* **2019**, *252*, 274–282.
- (9) Park, Y.; Runkle, E. S. Spectral-conversion film potential for greenhouses: Utility of green-to-red photons conversion and far-red filtration for plant growth. *PLoS One* **2023**, *18*, No. e0281996.
- (10) Shen, L.; Lou, R.; Park, Y.; Guo, Y.; Stallknecht, E. J.; Xiao, Y.; Rieder, D.; Yang, R.; Runkle, E. S.; Yin, X. Increasing greenhouse production by spectral-shifting and unidirectional light-extracting photonics. *Nature Food* **2021**, *2*, 434–441.
- (11) Protesescu, L.; Yakunin, S.; Bodnarchuk, M. I.; Krieg, F.; Caputo, R.; Hendon, C. H.; Yang, R. X.; Walsh, A.; Kovalenko, M. V. Nanocrystals of Cesium Lead Halide Perovskites (CsPbX₃, X = Cl, Br, and I): Novel Optoelectronic Materials Showing Bright Emission with Wide Color Gamut. *Nano Lett.* **2015**, *15*, 3692–3696.
- (12) Van der Laan, M.; de Weerd, C.; Poirier, L.; van de Water, O.; Poonia, D.; Gomez, L.; Kinge, S.; Siebbeles, L. D.; Koenderink, A. F.; Gregorkiewicz, T.; Schall, P. Photon Recycling in CsPbBr₃ All-Inorganic Perovskite Nanocrystals. *ACS Photonics* **2021**, *8*, 3201–3208.
- (13) Davis, N. J. L. K.; de la Pena, F. J.; Tabachnyk, M.; Richter, J. M.; Lamboll, R. D.; Booker, E. P.; Wisnivesky Rocca Rivarola, F.; Griffiths, J. T.; Ducati, C.; Menke, S. M.; Deschler, F.; Greenham, N. C. Photon Reabsorption in Mixed CsPbCl₃/CsPbI₃ Perovskite Nanocrystal Films for Light-Emitting Diodes. *J. Phys. Chem. C* **2017**, *121*, 3790–3796.
- (14) DuBose, J. T.; Kamat, P. V. Directing energy transfer in halide perovskite-chromophore hybrid assemblies. *J. Am. Chem. Soc.* **2021**, *143*, 19214–19223.

(15) DuBose, J. T.; Kamat, P. V. Energy Versus Electron Transfer: Managing Excited-State Interactions in Perovskite Nanocrystal-Molecular Hybrids. *Chem. Rev.* **2022**, *122*, 12475–12494.

(16) DuBose, J. T.; Kamat, P. V. How Pendant Groups Dictate Energy and Electron Transfer in Perovskite–Rhodamine Light Harvesting Assemblies. *J. Am. Chem. Soc.* **2023**, *145*, 4601–4612.

(17) Chemmangat, A.; Chakkamalayath, J.; DuBose, J. T.; Kamat, P. V. Tuning Energy Transfer Pathways in Halide Perovskite–Dye Hybrids through Bandgap Engineering. *J. Am. Chem. Soc.* **2024**, *146*, 3352–3362.

(18) Bansal, P.; Kar, P. Probing the energy transfer process by controlling the morphology of $\text{CH}_3\text{NH}_3\text{PbBr}_3$ nanocrystals with rhodamine B dye. *J. Lumin.* **2019**, *215*, No. 116609.

(19) Muthu, C.; Vijayan, A.; Nair, V. C. $\text{CH}_3\text{NH}_3\text{PbBr}_3$ Perovskite Nanocrystals as Efficient Light-Harvesting Antenna for Fluorescence Resonance Energy Transfer. *Chemistry - An Asian Journal* **2017**, *12*, 988–995.

(20) Rossi, A.; Price, M. B.; Hardy, J.; Gorman, J.; Schmidt, T. W.; Davis, N. J. Energy Transfer between Perylene Diimide Based Ligands and Cesium Lead Bromide Perovskite Nanocrystals. *J. Phys. Chem. C* **2020**, *124*, 3306–3313.

(21) Feld, L. G.; Boehme, S. C.; Morad, V.; Sahin, Y.; Kaul, C. J.; Dirin, D. N.; Rainò, G.; Kovalenko, M. V. Quantifying Förster Resonance Energy Transfer from Single Perovskite Quantum Dots to Organic Dyes. *ACS Nano* **2024**, *18*, 9997–10007.

(22) Cortes-Villena, A.; Bellezza, D.; Cunha, C.; Rosa-Pardo, I.; Seijas-Da Silva, A.; Pina, J.; Abellan, G.; Seixas de Melo, J. S.; Galian, R. E.; Perez-Prieto, J. Engineering Metal Halide Perovskite Nanocrystals with BODIPY Dyes for Photosensitization and Photocatalytic Applications. *J. Am. Chem. Soc.* **2024**, *146*, 14479–14492.

(23) Hoffman, J. B.; Choi, H.; Kamat, P. V. Size-Dependent Energy Transfer Pathways in CdSe Quantum Dot–Squaraine Light-Harvesting Assemblies: Förster versus Dexter. *J. Phys. Chem. C* **2014**, *118*, 18453–18461.

(24) Gorman, J.; Pandya, R.; Allardice, J. R.; Price, M. B.; Schmidt, T. W.; Friend, R. H.; Rao, A.; Davis, N. J. L. K. Excimer Formation in Carboxylic Acid-Functionalized Perylene Diimides Attached to Silicon Dioxide Nanoparticles. *J. Phys. Chem. C* **2019**, *123*, 3433–3440.

(25) Lu, H.; Schöps, O.; Woggon, U.; Niemeyer, C. M. Self-Assembled Donor Comprising Quantum Dots and Fluorescent Proteins for Long-Range Fluorescence Resonance Energy Transfer. *J. Am. Chem. Soc.* **2008**, *130*, 4815–4827.

(26) Hofmann, F. J.; Bodnarchuk, M. I.; Dirin, D. N.; Vogelsang, J.; Kovalenko, M. V.; Lupton, J. M. Energy Transfer from Perovskite Nanocrystals to Dye Molecules Does Not Occur by FRET. *Nano Lett.* **2019**, *19*, 8896–8902.

(27) Förster, T. Zwischenmolekulare Energiewanderung und Fluoreszenz. *Annalen der Physik* **1948**, *437*, 55–75.

(28) Li, S.; Ji, L.; Shi, Q.; Wu, H.; Fan, J. Advances in the production of bioactive substances from marine unicellular microalgae *Porphyridium* spp. *Bioresour. Technol.* **2019**, *292*, No. 122048.



CAS BIOFINDER DISCOVERY PLATFORM™

ELIMINATE DATA SILOS. FIND WHAT YOU NEED, WHEN YOU NEED IT.

A single platform for relevant, high-quality biological and toxicology research

Streamline your R&D

CAS
A Division of the American Chemical Society